Point Cloud Super Resolution with Adversarial Residual Graph Networks

Huikai Wu   Junge Zhang   Kaiqi Huang
Institute of Automation, Chinese Academy of Sciences
University of Chinese Academy of Sciences
{huikai.wu, jgzhang, kaiqi.huang}@nlpr.ia.ac.cn

Abstract

Point cloud super-resolution is a fundamental problem for 3D reconstruction and 3D data understanding. It takes a low-resolution (LR) point cloud as input and generates a high-resolution (HR) point cloud with rich details. In this paper, we present a data-driven method for point cloud super-resolution based on graph networks and adversarial losses. The key idea of the proposed network is to exploit the local similarity of point cloud and the analogy between LR input and HR output. For the former, we design a deep network with graph convolution. For the latter, we propose to add residual connections into graph convolution and introduce a skip connection between input and output. The proposed network is trained with a novel loss function, which combines Chamfer Distance (CD) and graph adversarial loss. Such a loss function captures the characteristics of HR point cloud automatically without manual design. We conduct a series of experiments to evaluate our method and validate the superiority over other methods. Results show that the proposed method achieves the state-of-the-art performance and have a good generalization ability to unseen data. Code is available at https://github.com/wuhuikai/PointCloudSuperResolution.

1. Introduction

When modeling an object from the real world for 3D printing or animation, a common way is to first obtain the point cloud with depth scanning devices or 3D reconstruction algorithms [7, 11] and then recover the mesh from the point cloud [3]. However, the captured point cloud is usually sparse and noisy due to the restrictions of devices or the limitations of algorithms, which leads to a low-quality mesh.

The key to improving the quality of the recovered mesh is point cloud super-resolution, which takes a LR point cloud as input and generates a HR point cloud with rich details and few noisy points, as shown in Figure 1. Most existing methods are optimization based without learning from
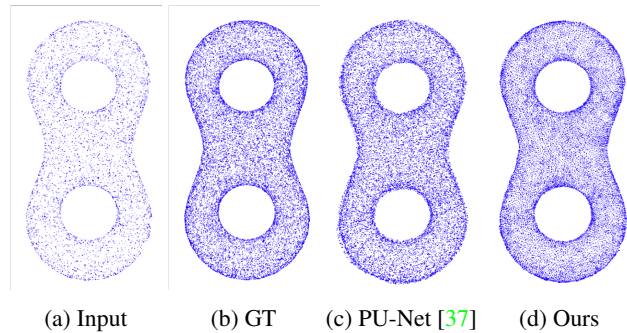

Figure 1: **Point Cloud Super Resolution.** (a) is the input LR point cloud with sparse distribution. (b) is the corresponding HR point cloud with dense distribution. (c) and (d) are the HR point cloud generated by PU-Net [37] and our method respectively. Ours is sharper at edges with fewer noisy points. Best viewed in color.

data, which have strong assumptions about the underlying surface of the HR point cloud [12, 13]. As for data-driven methods, few prior works study deep learning on this problem. [37] propose PU-Net for point cloud super-resolution, which is a pioneering work. By employing deep neural networks, it outperforms many traditional methods such as EAR [13] and achieves the state-of-the-art performance.

In this paper, we aim to advance the performance of point cloud super-resolution by overcoming the defects of PU-Net. The first problem is that PU-Net directly regresses the point coordinates without exploiting the similarity between LR and HR point cloud, which makes it hard to train. The second problem is that PU-Net proposes a complicated loss function with a strong assumption on the uniform distribution of HR point cloud. Manually designed loss functions tend to overfit human priors, which fail to capture many other properties of HR point cloud, such as continuity.

Recent work [16] in image super-resolution shows that predicting the residual between the LR and HR image is a more desirable way to achieve better accuracy. Thus, to solve the first problem, we propose to introduce residual connections into graph convolution networks (GCNs) [5]

and add a skip connection between the input layer and the output layer. Employing GCNs to process point cloud is not new [38]. However, the GCN in our method is unique in two aspects compared to that in [38]: (1) The architecture of our GCN is designed for generating point cloud while that in [38] aims at aggregating information for classification. (2) We propose an un-pooling layer for the GCN to upsample the input point cloud.

To solve the second problem, we design a graph adversarial loss based on LS-GAN [23]. The proposed loss function is more expressive than manually designed ones, which can capture the characteristics of HR point cloud automatically. Pan *et al*. also introduce adversarial loss into graph networks [25]. However, they focus on learning the distribution of graph embeddings. Thus, a multi-layer perceptron is employed as the discriminator to process the input vector. Differently, we aim at distinguishing real and fake point clouds. To achieve this, we propose a GCN as the discriminator to process the generated point cloud, which is significantly different from [25].

In this way, we propose a novel method for point cloud super-resolution, named Adversarial Residual Graph Convolution Network (AR-GCN). Experiments show that the proposed method achieves the state-of-the-art performance on both seen dataset [37] and unseen dataset (SHREC15). The contributions of our method are three-folds. First, we propose a novel architecture for point cloud super-resolution. Second, we introduce the graph adversarial loss to replace manually designed loss functions. Third, we advance the state-of-the-art performance on both seen and unseen datasets.

2. Related Work

2.1. Point Cloud Super Resolution

Point cloud super-resolution is formulated as an optimization problem in most earlier works. To upsample a point cloud, [2] first compute the Voronoi diagram on the moving least squares surface and then add points at the vertices of this diagram. [22] present a locally optimal projection operator for surface approximation based on L_1 median, which is parameter-free and robust to noisy points. These methods have a strong assumption on the smoothness of the underlying surface, which tend to have vague edges. Thus, [13] introduce an edge-aware point cloud upsampling method, which first samples away from the edges and then progressively samples the point cloud while approaching the edge singularities.

However, all these methods have strong assumptions about the underlying surface based on human priors. To exploit the massive 3D data, [37] propose a data-driven method that first learns multi-level features per point with PointNet++ [27] and then expands the point set via a multi-

branch convolution. Through end-to-end learning, this method outperforms the optimization based methods on multiple datasets, which achieves the state-of-the-art performance.

2.2. Deep Learning for 3D Data

There is a rising interest in 3D data processing recently. Most existing works transform 3D data into volumetric grids, which are then processed by 3D CNNs [30, 24, 36, 28]. Particularly, [30] propose to upsample 3D objects in voxel space, which is similar to point cloud super-resolution.

3D CNNs are memory and time consuming. Thus, following works propose to process point cloud directly instead of the volumetric grid [26, 27, 20, 32, 19, 14]. [26] propose a point-wise network for 3D object classification and segmentation. Successively, [27] introduce a hierarchical feature learning architecture to capture local and global context. [20] introduce a convolution operator named X-conv that is capable of leveraging spatially-local correlation for point cloud classification.

Besides 3D scene understanding, multiple works focus on employing deep learning for single image 3D reconstruction [7, 34, 33, 15]. [7] present a conditional shape sampler to generate multiple plausible point clouds from a single image. Differently, [34] propose a graph CNN for producing the 3D triangular mesh from a single color image.

2.3. Image Super Resolution

Super-resolution for 2D images is a well-studied problem, which is closely related to point cloud super-resolution. Modern approaches are usually built on deep learning in a data-driven manner [6, 35, 18, 39, 9, 10]. [6] first upsample the low-resolution image with bicubic interpolation and then use a shallow CNN to recover the details and textures. Instead of manually designed interpolation, [35] propose to jointly learn the interpolation and detail recovery. To generate realistic images, [18] present a generative adversarial network, which pushes the generated images close to natural images.

3. Method

In this section, we first define point cloud super-resolution formally and then introduce our method AR-GCN in detail. Our method is a novel approach that contains three major components: the adaptive adversarial loss function L_G, the residual GCN G, and the graph discriminator D. As shown in Figure 2, the LR point cloud x is directly fed into G to generate the HR output $\hat{y}$. Then, $\hat{y}$ is sent into D to produce L_G, while another loss L_{cd} is calculated based on $\hat{y}$ and the ground truth y.
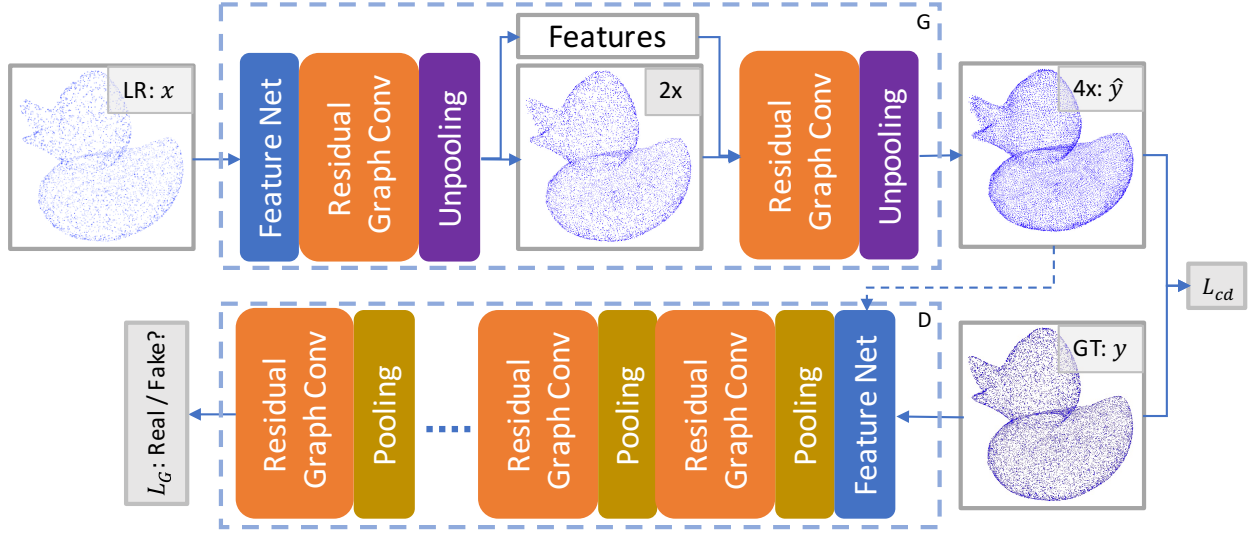
Figure 2: **Framework Overview.** The proposed AR-GCN consists of a generator G and a discriminator D. G is a residual GCN that upsamples the input point cloud progressively with the upsampling ratio $2\times$. D is also a residual GCN, which learns to distinguish fake HR point cloud from the real one.

3.1. Point Cloud Super Resolution

Formally, given a point cloud x with shape $n \times 3$, the goal of point cloud super-resolution is to generate a point cloud $\hat{y}$ with shape $N \times 3$ ($N = \gamma n, \gamma > 1$). Each point of $\hat{y}$ lies on the underlying surface described by x, as shown in Figure 1.

3.2. Method Overview: AR-GCN

As shown in Figure 2, our method AR-GCN consists of two networks, the generator G and the discriminator D. G aims to generate the HR point cloud by upsampling the LR input progressively, while D is responsible for distinguishing the fake HR point cloud from the real one. To train G and D simultaneously, we propose a joint loss function as shown in Equation 1:

$$L(x, y) = \lambda L_{cd}(G(x), y) + L_G(G(x)), \quad (1)$$

where λ controls the balance between L_{cd} and L_G.

L_{cd} measures the distance between y and $\hat{y}$, which is similar to L_2 loss in image super-resolution. As shown in Equation 2:

$$L_{cd}(\hat{y}, y) = \Sigma_{p \in y} min_{q \in \hat{y}} ||p - q||_2^2, \quad (2)$$

which is a variant of Chamfer Distance. The original Chamfer Distance consists of two parts: L_{cd} and $L_{\hat{cd}}$, where $L_{\hat{cd}}$ is symmetric with L_{cd} and defined as Equation 3:

$$L_{\hat{cd}}(\hat{y}, y) = \Sigma_{q \in \hat{y}} min_{p \in y} ||p - q||_2^2. \quad (3)$$

$L_{\hat{cd}}$ encourages $\hat{y}$ to be identical to the LR input, which leads to duplication points in the output point cloud. Thus, we remove $L_{\hat{cd}}$ and only employ L_{cd} as our loss function.

L_{cd} measures the point-wise distance between y and $\hat{y}$, which ignores high-order properties defined by a cluster of points, such as continuity. Traditional methods usually manually design a complex function as the loss, which is inefficient and has strong assumptions about the underlying surface. Alternatively, we propose a loss function L_G that is defined by a network and learned from data automatically. Concretely, L_G is a graph adversarial loss that is inspired by generative adversarial networks (GANs) [8]. In this paper, we employ LS-GAN [23] as the adversarial loss for its simplicity and effectiveness. L_G is defined as follows:

$$L_G(\hat{y}) = ||1 - D(\hat{y})||_2^2, \quad (4)$$

where D is the discriminator that aims to distinguish real and fake HR point cloud by minimizing the following loss:

$$L_D(\hat{y}, y) = \frac{1}{2}||D(\hat{y})||_2^2 + \frac{1}{2}||1 - D(y)||_2^2. \quad (5)$$

3.3. Residual Graph Convolution Generator

The generator G is built on the Graph Convolution Network (GCN) [4], which aims to progressively upsample the LR point cloud. It consists of three building blocks, namely residual graph convolution block, unpooling block and feature net, as shown in Figure 2.

3.3.1 Residual Graph Convolution Block

PU-Net employs PointNet++ to generate HR point cloud, which treats the central point and the neighbor points equally. This limits the learning ability of the network. Alternatively, we build our method on graph convolution [4], as shown in Figure 3.
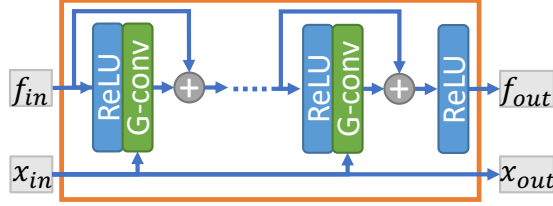
Figure 3: **Residual Graph Convolution Block.** x_{in} is used for querying the k nearest neighbors. x_{out} is the same as x_{in}.

The core of graph convolution, G-conv, is defined on a graph G=(υ, ε) and calculated as follows,

$$f_{l+1}^p = w_0 f_l^p + w_1 \Sigma_{q \in N(p)} f_l^q, \forall p \in \upsilon, \quad (6)$$

where w is the learn-able parameters and f_l^p represents the feature of vertex p at layer l. $N(p)$ is the vertices that connect to p as defined by the adjacency matrix ε. However, there's no predefined adjacency matrix for a point cloud. To solve this problem, we define $N(p)$ as the k nearest neighbors of p in Euclidean space, of which the coordinates are defined by x_{in}.

Besides G-conv, we also introduce residual connections into our block, because residual networks usually lead to faster convergence and better results. It also helps to exploit the similarity between LR point cloud and the corresponding HR point cloud.

In our experiment, the number of neighbors k is set to 8. All the G-conv operators inside the block have the same number of channels, which is 128. The input feature f_{in} and point cloud x_{in} are processed by 12 residual layers to obtain f_{out}, while x_{out} is the same as x_{in}.

3.3.2 Unpooling Block

The unpooling block takes point cloud x_{in} and the corresponding features f_{in} as inputs. It first transforms f_{in} with shape $\hat{n} \times c$ to a tensor with shape $\hat{n} \times 6$ by a G-conv layer. The tensor is then reshaped to $\hat{n} \times 2 \times 3$, which is noted as δx. The upsampled point cloud x_{out} is obtained by adding x_{in} and δx point-wisely, where each point is transformed into 2 points. The unpooling block is designed to predict the residual between x_{in} and x_{out} instead of regressing x_{out} directly. This exploits the similarity between x_{in} and x_{out}, which leads to a faster convergence and better performance.

The feature of the output point cloud, f_{out}, are obtained by the following equation:

$$f_{out}^p = \frac{1}{k} \Sigma_{q \in N[x_{in}](p)} f_{in}^q, \forall p \in x_{out}, \quad (7)$$

where $N[x_{in}](p)$ means the k nearest neighbors of point p in point cloud x_{in}.

3.3.3 Feature Net

As shown in Figure 3, a residual graph convolution block takes both the point cloud and the corresponding feature as inputs. However, the generator only have one input, the point cloud x. To obtain the other input, the corresponding feature f, we design a simple block named feature net, which takes the point cloud x as input. Specifically, for each point $p \in x$ with shape 1×3, we first obtain its k nearest neighbors P with shape $k \times 3$. Then, a series of point-wise convolutions with a max-pooling layer transform $\hat{P} = P - p$ into f^p with shape $1 \times c$.

In our experiment, k is set to 8 while c is set to 128. The number of convolution layers is set to 3.

3.3.4 Progressive Super Resolution

Instead of directly upsampling the LR point cloud with the desired upscale ratio, we choose to generate the HR point cloud step by step. The point cloud is upsampled by 2 times at each step, as shown in Figure 2. Our experiment shows that such an approach results in better accuracy.

3.4. Graph Discriminator

To generate more realistic HR point cloud, we present a graph adversarial loss for point cloud, which is defined by the discriminator D. As shown in Figure 2, D is composed of feature net, residual graph convolution block, and pooling block. For feature net, k is set to 8 while c is set to 64. The number of convolution layers is set to 2. For residual graph convolution block, k is set to 8 while c is set to 64. The number of layers is set to 4.

Pooling Block Given the input point cloud x_{in} with shape $4n \times 3$, we first employ farthest point sampling (FPS) to generate x_{out} with shape $n \times 3$. The corresponding features f_{out} is then obtained as follows:

$$f_{out}^p = max_{q \in N[x_{in}](p)} f_{in}^q, \forall p \in x_{out}, \quad (8)$$

where max is applied element-wisely.

Graph Patch GAN Most discriminators downsample the input progressively to obtain a single flag for the whole input. Such a design usually leads to blurry and unpleasant artifacts. Instead of employing a global discriminator, we build a graph patch GAN based on [29]. Specifically, our discriminator downsamples the input multiple times so that the output contains more than 1 point. Graph patch GAN forces every local patch of the generated point cloud to lie on the distribution of the real HR point cloud. In our experiment, we set the number of the output points to 64.

4. Experiment

In this section, we first introduce the datasets for training and testing, as well as the details of our implementation.

Method	CD	EMD	F-score $\tau = 0.01$	NUC with different p					Deviation (1e-2)		Params
				0.2%	0.4%	0.6%	0.8%	1.0%	mean	std	
Input	0.0120	0.0036	41.33%	0.315	0.224	0.185	0.163	0.150	-	-	-
MLS [2]	0.0117	0.0043	57.70%	0.364	0.272	0.229	0.204	0.186	**0.18**	0.34	-
PU-Net [37]	0.0118	0.0041	43.24%	0.206	0.165	0.147	0.137	0.131	0.78	0.66	**0.777M**
AR-GCN	**0.0084**	**0.0035**	**70.28%**	**0.204**	**0.164**	**0.145**	**0.134**	**0.128**	0.26	**0.30**	0.785M

Table 1: **Quantitative Comparison on the Train-Test Dataset.**

Method	CD	EMD	F-score $\tau = 0.01$	NUC with different p					Deviation (1e-2)	
				0.2%	0.4%	0.6%	0.8%	1.0%	mean	std
Input	0.0077	**0.0031**	27.86%	0.310	0.220	0.183	0.163	0.151	-	-
MLS [2]	0.0067	0.0032	84.69%	0.253	0.199	0.173	0.159	0.150	0.33	0.46
PU-Net [37]	0.0103	0.0050	56.39%	0.283	0.230	0.204	0.189	0.180	0.90	0.73
AR-GCN	**0.0054**	**0.0031**	**93.07%**	**0.201**	**0.162**	**0.144**	**0.135**	**0.130**	**0.18**	**0.19**

Table 2: **Quantitative Comparison on SHREC15.**

The quantitative and qualitative results are then presented to show the effectiveness of our method. To demonstrate the effect of each component in AR-GCN, we also conduct a comprehensive ablation study. To further show the potential applications of our method, we test AR-GCN in an iterative setting and apply it to 3D reconstruction task. Besides, we also employ our method to assist LR point cloud classification.

4.1. Datasets

We utilize two datasets for our experiments. One is the train-test dataset, which our method is trained with and tested on. The other is the unseen dataset, where our method is directly tested without training or finetuning.

Train-Test Dataset We use the dataset proposed in PU-Net [37] for training and testing. This dataset contains 60 different models from the Visionair repository. Following the protocol in PU-Net, we use 40 models for training while the other 20 models are used for testing. For training, 100 patches are extracted from each model as the ground truth, which contains 4, 096 points. The input patch is randomly sampled from the ground truth patch at each iteration of training, which contains 1, 024 points. For testing, we sample 20, 000 points uniformly per model as the ground truth, while sampling 5, 000 points as the input.

Unseen Dataset: SHREC15 To further validate the generalization ability of our method, we directly test AR-GCN on SHREC15 [21] after training with the train-test dataset without finetuning. For SHREC15, there are 50 categories in total and 24 models in each category. We randomly choose one model from each category for testing, since the models in each category only differ in the pose. Same as the train-test dataset, the ground truth contains 20, 000 points, while the input contains 5, 000 points.

4.2. Implementation Details

Our method is implemented in Tensorflow [1] and runs on a single Titan-Xp GPU. To avoid overfitting, we augment the training data by randomly rotating, shifting and scaling the data. For optimization, we use Adam [17] as the optimizer, where the batch size is 28 and the learning rate is 0.001. The network is firstly trained with L_{cd} for 80 epochs at the speed of 2.2 min/epoch. Then we add L_G and finetune the network for another 40 epochs at the speed of 4.9 min/epoch. The training process takes about 6.2 hours in total, while it takes about 4.8 hours for training PU-Net under the same setting (2.4 min/epoch).

4.3. Quantitative Results

Evaluation Metrics We adopt standard 3D reconstruction metrics for point cloud super-resolution because the output of both tasks is point cloud. To measure the difference between $\hat{y}$ and y point-wisely, we utilize the standard Chamfer Distance (CD) and Earth Mover's Distance (EMD), for which smaller is better.

CD and EMD are heavily influenced by the outliers. Thus, we also report F-score [31] by treating point cloud super-resolution as a classification problem. Specifically, precision and recall are first evaluated by checking the percentage of points in $\hat{y}$ or y that can find a neighbor from the other within certain threshold τ. The F-score is then calculated as the harmonic mean of precision and recall. For this metric, larger is better.

The metrics in [37] are also employed to evaluate our method. We use Deviation to measure the difference between the predicted point cloud and the ground truth mesh, while normalized uniformity coefficient (NUC) is evaluated for measuring the uniformity. For these two metrics, smaller is better. Notably, the original mesh is used as the ground truth instead of the sampled 20, 000 points.

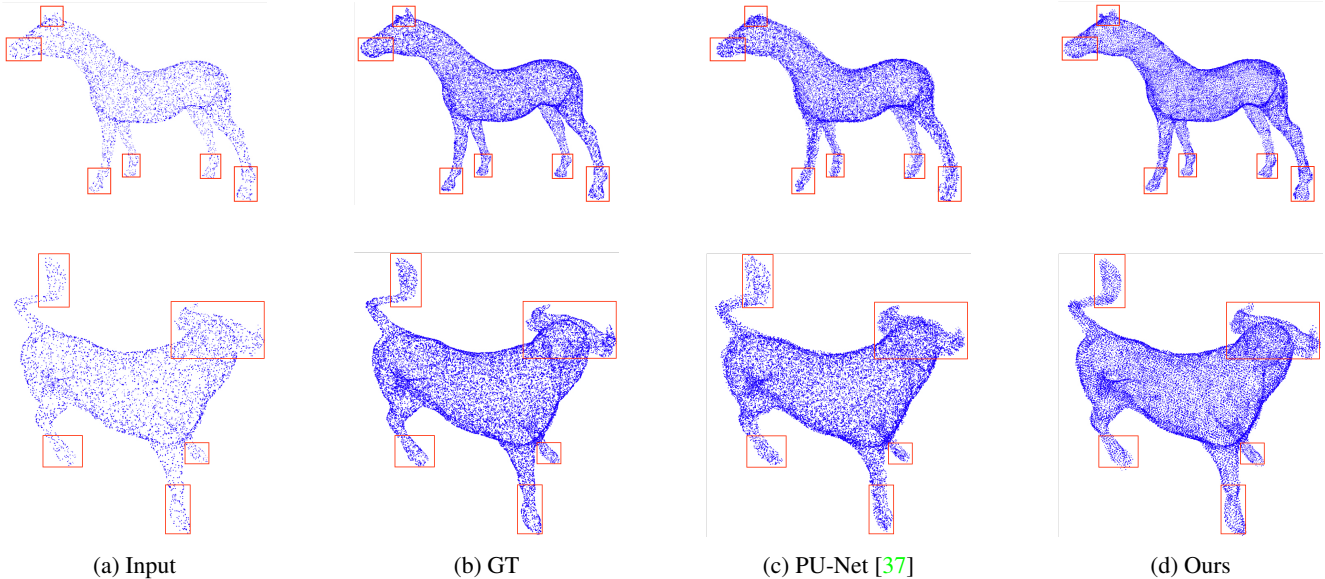|			
(a) Input	(b) GT	(c) PU-Net [37]	(d) Ours

Figure 4: **Qualitative Results.** (a) is the LR input point cloud with a sparse distribution, while (b) is the corresponding HR point cloud with a dense distribution. (c) and (d) are the HR point cloud generated by PU-Net [37] and our method. Our results are sharper at edges, which have richer details but fewer noisy points, especially in the red boxes. Best viewed in color.

Method	Train-Test Dataset					SHREC15				
	CD	EMD	F-score	Deviation (1e-2)		CD	EMD	F-score	Deviation (1e-2)	
			$\tau = 0.01$	mean	std			$\tau = 0.01$	mean	std
$GCN^{4\times}_{points}$	0.0971	0.0857	3.96%	13.7	12.3	0.0925	0.0778	8.03%	10.3	10.1
$GCN^{4\times}$	0.0092	0.0036	63.79%	0.31	0.35	0.0061	0.0031	87.98%	0.24	0.27
$ResGCN^{4\times}$	0.0090	0.0036	65.04%	0.36	0.37	0.0059	0.0031	90.57%	0.25	0.25
PU-Net [37]	0.0118	0.0041	43.24%	0.78	0.66	0.0103	0.0050	56.39%	0.90	0.73
ResGCN	0.0086	**0.0035**	68.75%	0.30	0.31	0.0056	0.0031	92.32%	0.21	0.21
$ResGCN + L_{pu}$	0.0096	0.0040	60.71%	0.36	0.50	0.0064	0.0031	86.46%	0.26	**0.14**
AR-GCN w/o FT	0.0085	0.0041	69.53%	0.27	**0.30**	0.0055	**0.0027**	92.46%	**0.18**	0.19
AR-GCN	**0.0084**	**0.0035**	**70.28%**	**0.26**	**0.30**	**0.0054**	0.0030	**93.07%**	**0.18**	0.19

Table 3: **Ablation Study Results on the Train-Test Dataset and the Unseen Dataset, SHREC15.**

Comparison with Other Methods The performance of different methods on the train-test dataset is reported in Table 1. We first report the performance of the LR input as a preliminary baseline. We then report the performance of Moving Least Squares (MLS) [2], which is a traditional method.[1] The performance of PU-Net is then reported, which is the state-of-the-art method for point cloud super-resolution.[2]

As shown in Table 1, our method outperforms all the other methods under most metrics. Particularly, our method improves the F-score by more than 10%, while advances CD a large step. Surprisingly, our method even outperforms PU-Net in NUC, although it is not trained with the repulsion loss [37], which forces the generated point cloud uniform.

We attribute this to the effect of our adversarial loss. As for MLS, it performs well in Deviation but has the lowest NUC scores. The reason is that MLS tends to produce new points close to the points in the input point cloud, which leads to a non-uniformly distributed point cloud, resulting in poor performance on NUC metric. However, the mean deviation to the ground truth is small. Similar results are obtained on SHREC15 as shown in Table 2, which shows the generalization ability of our method on the unseen dataset. As for NUC and Deviation, our method outperforms the baseline methods by a large margin.

Since both our method and PU-Net are deep learning based method, we also compare the number of parameters in each model. As shown in Table 1, our model contains about the same number of learnable parameters as PU-Net while achieves much better performance.

---

[1] The result of MLS is reproduced with Point Cloud Library (PCL).

[2] The result of PU-Net is reproduced with the official code by following the author's instructions.

4.4. Qualitative Results

The evaluation metrics reflect the shape quality to some degree. However, they mainly focus on point-wise distance and fail to reflect the surface properties such as smoothness and high-order details. Since there are barely any standard metrics to measure these aspects, we present a series of qualitative results to show the advantage of our method.

Figure 4 presents the point clouds in both datasets visually, where the 1st row is from the train-test dataset and the 2nd row is from SHREC15. Compared to PU-Net, the HR point clouds of our method have richer details and sharper edges. Besides, ours are more uniformly distributed in the smooth area with fewer noisy points. On the contrary, the results from PU-Net are noisy and blurry on the edges with little details. It tends to outspread uniformly without preserving the underlying structure. Notably, the differences around the legs, feet and horns are most obvious, as shown in the red boxes.

4.5. Ablation Study

To further verify the effect of each component in our method, we conduct an ablation study on both datasets and present the results in Table 3.

We first present the results of a very simple baseline $GCN_{points}^{4\times}$. Compared to AR-GCN, there are mainly three modifications. First, we remove the residual connections from the proposed generator, as well as the skip connection between input and output. Second, it regresses the coordinates directly under the supervision of a single loss L_{cd}. Third, instead of progressively upscaling, it upsamples the point cloud by $4\times$ directly with the number of G-conv layers unchanged. Without all the key features in our method, it is not surprising that this simple baseline does not work at all. We then put back the skip connection between input and output, which forces the model to predict the residual δx instead of directly regressing the point coordinates. This simple change largely improves the stability of learning, which results in a model with a reasonable performance, as shown by $GCN^{4\times}$. We further transform graph convolution into residual graph convolution by putting back the residual connections. Such a modification improves F-score by about 3% on SHREC15 and 1.5% on the train-test dataset, as shown by $ResGCN^{4\times}$. By enabling progressive super-resolution, we obtain the proposed generator. As shown by ResGCN, the F-score increases by nearly 4% on the train-test dataset. The Deviation also improves a lot on both datasets. When changing L_{cd} into the loss proposed in [37], the F-score decreases by about 8% as shown by ResGCN + L_{pu} and ResGCN, which demonstrates the effectiveness of L_{cd}. Compared to PU-Net, ResGCN + L_{pu} improves the F-score by more than 17% because of the proposed residual graph network ResGCN. By replacing L_{pu} with the proposed loss, the F-score is further improved by around 9%,

Dataset	Method	F-score $\tau = 0.01$	NUC 1.0%	Deviation mean
Train-Test	PU-Net	43.2%	0.131	0.78
	Ours	70.3%	0.128	0.26
	Ours+noisy	55.4%	0.128	0.59
	Ours+uneven	46.0%	0.202	0.56
SHREC15	PU-Net	56.4%	0.180	0.90
	Ours	93.1%	0.130	0.18
	Ours+noisy	78.8%	0.130	0.55
	Ours+uneven	75.5%	0.201	0.37

Table 4: **Experiments on noisy data and uneven data.**

which achieves the state-of-the-art performance, as shown by AR-GCN.

We also take an experiment to compare different training strategies. AR-GCN w/o FT is trained with the proposed loss $L(x, y)$ for 120 epochs, while AR-GCN is trained with L_{cd} for 80 epochs and then finetuned with $L(x, y)$ for another 40 epochs. As shown in the table, AR-GCN outperforms AR-GCN w/o FT consistently, which shows the superiority of the 2-step training strategy.

4.6. Robustness of AR-GCN

To show the robustness of our method, we take experiments on noisy point clouds and non-uniformly sampled point clouds separably. The quantitative results on the Train-Test dataset and SHREC15 are shown in Table 4. Ours+noisy represents applying AR-GCN on noisy point clouds (Gaussian noise z, where $z \sim \mathcal{N}(0, 0.01)$). Results show that our method with noisy point clouds outperforms PU-Net with clean ones. Ours+uneven means employing our method on non-uniformly sampled point clouds. Our method with uneven point clouds achieves similar performance to PU-Net with uniform ones on all the metrics except NUC. We attribute this to the non-uniform distribution of the input point clouds. Our method can only make it more uniform to a certain degree. We plan to solve this problem in the future work.

4.7. Applications

Iterative Super Resolution   Our method is trained to upscale a point cloud by a fixed ratio, which is $4\times$ in our setting. To demonstrate the ability of upsampling a point cloud by more than $4\times$, we conduct an experiment that takes the output of the previous iteration as input and upsamples it by $4\times$ again with AR-GCN. The initial point cloud has $1,024$ points, which are upsampled by $16\times$ after 2 iterations. As shown in Figure 5, our method not only handles a relatively sparse point cloud but also upsamples it by more than $4\times$ iteratively. Although the resulting point cloud is not as good as that in Figure 4, it recovers many details from the point cloud with only $1,024$ points, which is promising.
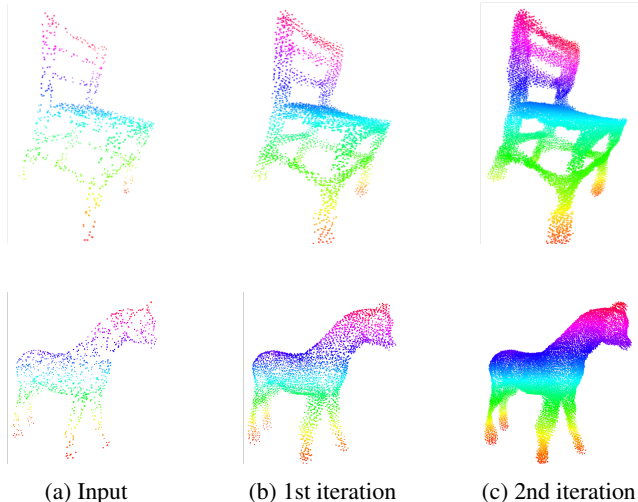
(a) Input   (b) 1st iteration   (c) 2nd iteration

Figure 5: **Iterative Super Resolution.** (a) is the input point cloud with $1,024$ points. (b) and (c) are the generated HR point clouds after the 1st and 2nd iterations. At each iteration, the output from the previous iteration is upsampled by 4 times with our method. Best viewed in color.
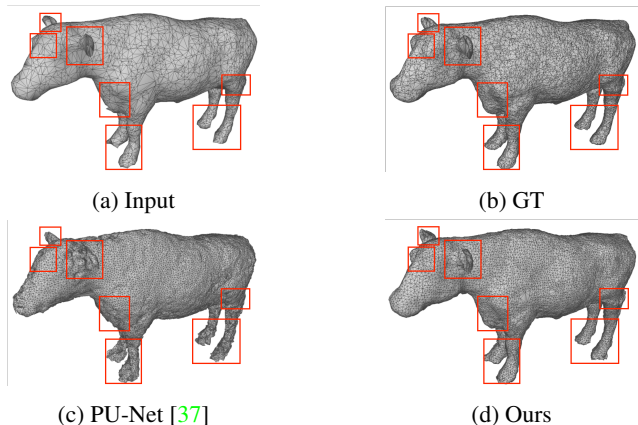

(a) Input   (b) GT

(c) PU-Net [37]   (d) Ours

Figure 6: **Mesh Reconstruction from Point Cloud.** The differences inside the red boxes are most obvious. Best viewed in color.

3D Reconstruction In 3D reconstruction, the quality and density of the point cloud have a huge impact on the quality of the reconstructed mesh. However, due to the limitations of scanning devices, the point cloud is usually sparse and noisy. Thus, point cloud super-resolution is the key to improve the quality of 3D reconstruction. We employ our method and PU-Net to generate the HR point cloud, which is then fed into Ball pivoting algorithm [3] for mesh reconstruction. As shown in Figure 6, the mesh reconstructed from our method contains richer details compared to that from the LR input. Besides, ours is smoother in the flat area and sharper at the edges, while the mesh from PU-Net is noisy with many unpleasant artifacts, especially in the red boxes.
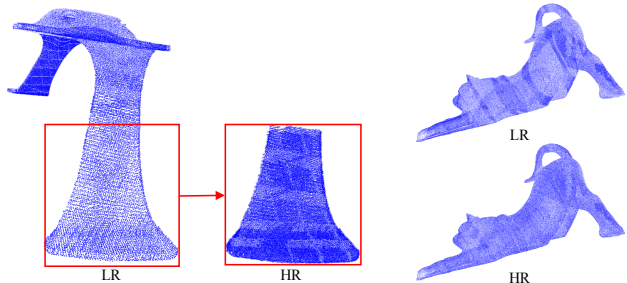

Figure 7: Employ our method on real-scanned and un-even point cloud. Best viewed in color.

#Points	1024	256	1024 (from 256 points)
Accuracy (%)	91.05	46.96	79.34

Table 5: Classification accuracy on the test set of Model-Net40 with PointNet++. 1024 (from 256 points) is obtained by upsampling the 256 points 4 times with our method.

LR Point Cloud Classification For 3D understanding, the classification accuracy of the LR point cloud is usually lower than that of the HR point cloud. To improve the performance of LR point cloud classification, one possible way is transforming it to HR point cloud with the point cloud super-resolution method. To show the effectiveness of point cloud super-resolution, we employ PointNet++ [27] on ModelNet40 dataset [36] for point cloud classification. As shown in Table 5, PointNet++ achieves 91.05% in classification accuracy with $1,024$ points as input. When we randomly sample 256 points from the $1,024$ points and send them to PointNet++, the performance drops from 91.05% to 46.96%. We then upsample the 256 points by $4\times$ with our method and send the $1,024$ points to PointNet++, resulting in 79.34% in accuracy, which outperforms 46.96% by a large margin. This experiment shows that point cloud super-resolution is important for understanding LR point cloud.

Real-Scanned Point Cloud We also conduct an experiment on real-scanned and un-even point clouds. As shown in Figure 7, our method generates a denser point cloud with more uniformly distributed points, while maintains the underlying structure such as the striped texture.

5. Conclusion

We proposed a graph convolution network AR-GCN for point cloud super-resolution, which is composed of a residual generator, a graph discriminator, and a graph adversarial loss. With comprehensive experiments, we demonstrated that residual connections and residual prediction are effective for stable training and better performance. With the proposed graph adversarial loss, our method generates more realistic HR point cloud compared to the manually designed loss function. The experiment on train-test dataset showed that our method outperforms other methods. The

experiment on the unseen dataset SHREC15 further demonstrated the better performance and generalization ability of our method. Notably, our method is not designed for completion, thus it can not fill large holes or missing parts. We'd like to solve the limitations in the future work.

References

[1] M. Abadi, P. Barham, J. Chen, Z. Chen, A. Davis, J. Dean, M. Devin, S. Ghemawat, G. Irving, M. Isard, et al. Tensorflow: a system for large-scale machine learning. In *OSDI*, 2016. 5

[2] M. Alexa, J. Behr, D. Cohen-Or, S. Fleishman, D. Levin, and C. T. Silva. Computing and rendering point set surfaces. *IEEE Transactions on visualization and computer graphics*, 2003. 2, 5, 6

[3] F. Bernardini, J. Mittleman, H. Rushmeier, C. Silva, and G. Taubin. The ball-pivoting algorithm for surface reconstruction. *IEEE transactions on visualization and computer graphics*, 1999. 1, 8

[4] M. M. Bronstein, J. Bruna, Y. LeCun, A. Szlam, and P. Vandergheynst. Geometric deep learning: going beyond euclidean data. *IEEE Signal Processing Magazine*, 2017. 3

[5] M. Defferrard, X. Bresson, and P. Vandergheynst. Convolutional neural networks on graphs with fast localized spectral filtering. In *NIPS*, 2016. 2

[6] C. Dong, C. C. Loy, K. He, and X. Tang. Learning a deep convolutional network for image super-resolution. In *ECCV*, 2014. 2

[7] H. Fan, H. Su, and L. J. Guibas. A point set generation network for 3d object reconstruction from a single image. In *CVPR*, 2017. 1, 2

[8] I. Goodfellow, J. Pouget-Abadie, M. Mirza, B. Xu, D. Warde-Farley, S. Ozair, A. Courville, and Y. Bengio. Generative adversarial nets. In *NIPS*, 2014. 3

[9] W. Han, S. Chang, D. Liu, M. Yu, M. Witbrock, and T. S. Huang. Image super-resolution via dual-state recurrent networks. In *CVPR*, 2018. 2

[10] M. Haris, G. Shakhnarovich, and N. Ukita. Deep backprojection networks for super-resolution. In *CVPR*, 2018. 2

[11] R. Hartley and A. Zisserman. *Multiple view geometry in computer vision*. Cambridge university press, 2003. 1

[12] H. Huang, D. Li, H. Zhang, U. Ascher, and D. Cohen-Or. Consolidation of unorganized point clouds for surface reconstruction. *TOG*, 2009. 1

[13] H. Huang, S. Wu, M. Gong, D. Cohen-Or, U. Ascher, and H. R. Zhang. Edge-aware point set resampling. *TOG*, 2013. 1, 2

[14] M. Jiang, Y. Wu, and C. Lu. Pointsift: A sift-like network module for 3d point cloud semantic segmentation. *arXiv:1807.00652*, 2018. 2

[15] H. Kato, Y. Ushiku, and T. Harada. Neural 3d mesh renderer. In *CVPR*, 2018. 2

[16] J. Kim, J. Kwon Lee, and K. Mu Lee. Deeply-recursive convolutional network for image super-resolution. In *CVPR*, 2016. 1

[17] D. P. Kingma and J. Ba. Adam: A method for stochastic optimization. *arXiv:1412.6980*, 2014. 5

[18] C. Ledig, L. Theis, F. Huszár, J. Caballero, A. Cunningham, A. Acosta, A. P. Aitken, A. Tejani, J. Totz, Z. Wang, et al. Photo-realistic single image super-resolution using a generative adversarial network. In *CVPR*, 2017. 2

[19] J. Li, B. M. Chen, and G. H. Lee. So-net: Self-organizing network for point cloud analysis. In *CVPR*, 2018. 2

[20] Y. Li, R. Bu, M. Sun, and B. Chen. Pointcnn. *arXiv:1801.07791*, 2018. 2

[21] Z. Lian, J. Zhang, S. Choi, H. ElNaghy, J. El-Sana, T. Furuya, A. Giachetti, R. A. Guler, L. Lai, C. Li, H. Li, F. A. Limberger, R. Martin, R. U. Nakanishi, A. P. Neto, L. G. Nonato, R. Ohbuchi, K. Pevzner, D. Pickup, P. Rosin, A. Sharf, L. Sun, X. Sun, S. Tari, G. Unal, and R. C. Wilson. Non-rigid 3d shape retrieval. In *3DOR*, 2015. 5

[22] Y. Lipman, D. Cohen-Or, D. Levin, and H. Tal-Ezer. Parameterization-free projection for geometry reconstruction. *TOG*, 2007. 2

[23] X. Mao, Q. Li, H. Xie, R. Y. Lau, Z. Wang, and S. P. Smolley. Least squares generative adversarial networks. In *ICCV*, 2017. 2, 3

[24] D. Maturana and S. Scherer. Voxnet: A 3d convolutional neural network for real-time object recognition. In *IROS*, 2015. 2

[25] S. Pan and etc. Adversarially regularized graph autoencoder for graph embedding. In *IJCAI*, 2018. 2

[26] C. R. Qi, H. Su, K. Mo, and L. J. Guibas. Pointnet: Deep learning on point sets for 3d classification and segmentation. *arXiv:1612.00593*, 2016. 2

[27] C. R. Qi, L. Yi, H. Su, and L. J. Guibas. Pointnet++: Deep hierarchical feature learning on point sets in a metric space. In *NIPS*, 2017. 2, 8

[28] G. Riegler, A. O. Ulusoy, and A. Geiger. Octnet: Learning deep 3d representations at high resolutions. In *CVPR*, 2017. 2

[29] A. Shrivastava, T. Pfister, O. Tuzel, J. Susskind, W. Wang, and R. Webb. Learning from simulated and unsupervised images through adversarial training. In *CVPR*, 2017. 4

[30] E. Smith, S. Fujimoto, and D. Meger. 3d object super-resolution. *arXiv:1802.09987*, 2018. 2

[31] M. Sokolova, N. Japkowicz, and S. Szpakowicz. Beyond accuracy, f-score and roc: a family of discriminant measures for performance evaluation. In *Australasian joint conference on artificial intelligence*, 2006. 5

[32] H. Su, V. Jampani, D. Sun, S. Maji, E. Kalogerakis, M.-H. Yang, and J. Kautz. Splatnet: Sparse lattice networks for point cloud processing. In *CVPR*, 2018. 2

[33] X. Sun, J. Wu, X. Zhang, Z. Zhang, C. Zhang, T. Xue, J. B. Tenenbaum, and W. T. Freeman. Pix3d: Dataset and methods for single-image 3d shape modeling. In *CVPR*, 2018. 2

[34] N. Wang, Y. Zhang, Z. Li, Y. Fu, W. Liu, and Y.-G. Jiang. Pixel2mesh: Generating 3d mesh models from single rgb images. *arXiv:1804.01654*, 2018. 2

[35] Y. Wang, L. Wang, H. Wang, and P. Li. End-to-end image super-resolution via deep and shallow convolutional networks. *arXiv:1607.07680*, 2016. 2

[36] Z. Wu, S. Song, A. Khosla, F. Yu, L. Zhang, X. Tang, and J. Xiao. 3d shapenets: A deep representation for volumetric shapes. In *CVPR*, 2015. 2, 8

[37] L. Yu, X. Li, C.-W. Fu, D. Cohen-Or, and P.-A. Heng. Punet: Point cloud upsampling network. In *CVPR*, 2018. 1, 2, 5, 6, 7, 8

[38] Y. Zhang and M. Rabbat. A graph-cnn for 3d point cloud classification. In *ICASSP*, 2018. 2

[39] Y. Zhang, Y. Tian, Y. Kong, B. Zhong, and Y. Fu. Residual dense network for image super-resolution. In *CVPR*, 2018. 2